RSC Advances

PAPER

View Article Online
View Journal | View Issue

Check for updates

Cite this: *RSC Adv.*, 2023, **13**, 7000

Covalent functionalization of graphene sheets for plasmid DNA delivery: experimental and theoretical study

Mohyeddin Assali, *[a] Naim Kittana, *[b] Ismail Badran [c] and Safa Omari[a]

Several approaches, including plasmid transfection and viral vectors, were used to deliver genes into cells for therapeutic and experimental purposes. However, due to the limited efficacy and questionable safety issues, researchers are looking for better new approaches. Over the past decade, graphene has attracted tremendous attention in versatile medical applications, including gene delivery, which could be safer than the traditional viral vectors. This work aims to covalently functionalize pristine graphene sheets with a polyamine to allow the loading of plasmid DNA (pDNA) and enhance its delivery into cells. Graphene sheets were successfully covalently functionalized with a derivative of tetraethylene glycol connected to polyamine groups to improve their water dispersibility and capacity to interact with the pDNA. The improved dispersibility of the graphene sheets was demonstrated visually and by transmission electron microscopy. Also, it was shown by thermogravimetric analysis that the degree of functionalization was about 58%. Moreover, the surface charge of the functionalized graphene was +29 mV as confirmed by zeta potential analysis. The complexion of f-graphene with pDNA was achieved at a relatively low mass ratio (10 : 1). The incubation of HeLa cells with f-graphene loaded with pDNA that encodes enhanced green fluorescence protein (eGFP) resulted in the detection of fluorescence signal in the cells within one hour. f-Graphene showed no toxic effect *in vitro*. Density functional theory (DFT) and quantum theory of atoms in molecules (QTAIM) calculations revealed strong binding with $\Delta H_{298} = 74.9$ kJ mol^{-1}. QTAIM between the f-graphene and a simplified model of pDNA. Taken together, the developed functionalized graphene could be used for the development of a new non-viral gene delivery system.

Received 2nd February 2023
Accepted 22nd February 2023

DOI: 10.1039/d3ra00727h

rsc.li/rsc-advances

Open Access Article. Published on 02 March 2023. Downloaded on 1/31/2025 1:53:19 PM.
This article is licensed under a Creative Commons Attribution-NonCommercial 3.0 Unported Licence.

1. Introduction

Gene therapy is emerging as a new class of therapeutics for the treatment of many inherited and acquired incurable diseases. It is a rapidly growing and promising field of medical research that involves the delivery of genes that encode proteins aimed to correct specific deficits within diseased cells.[1] Viral vectors have been used successfully over the past few decades to deliver genes into cells for research purposes. Although a few viral vector-based drugs recently received approval from the regulatory authorities to treat certain types of cancers and monogenic diseases, there are still real concerns regarding their safety due to potential *in vivo* mutagenicity, the probability to induce severe immune reactions, and several other health hazards. Therefore, there is a demand for developing safer alternatives.[2–4]

Carbon-based nanomaterials possess interesting physical, mechanical, and chemical properties that enable their versatile use in various biomedical fields.[5–7] Graphene sheets constitute a class of carbon allotropes with a two-dimensional (sheet-like) structure with a large surface area that is proposed to load a large number of therapeutic molecules, rendering it as an attractive candidate for drug and gene delivery.[8] Graphene and its derivatives have been used for biomedical purposes like drug delivery, gene delivery, biosensing, bioimaging, tissue engineering, and cancer therapy.[9] However, graphene is hydrophobic in nature and tends to form aggregates in most solvents.[10] Therefore, the potential application of graphene in the biological field implies the necessity to improve its dispersibility, especially in water, to be compatible with biological environments. An important approach to improve the dispersibility of graphene in water is by covalent or non-covalent functionalization with polar functional groups, likewise, the loading of drugs and nucleic acids.[11–13] Non-covalent functionalization could be achieved by polymer wrapping and adsorption of surfactants or small aromatic molecules. It usually involves decorating functional species onto graphene sheets *via* π–π stacking, hydrophobic attraction, hydrogen bonding and/or electrostatic interactions.[14,15] However, the noncovalent

[a]*Department of Pharmacy, Faculty of Medicine and Health Sciences, An-Najah National University, Nablus, Palestine. E-mail: m.d.assali@najah.edu*
[b]*Department of Biomedical Sciences, Faculty of Medicine and Health Sciences, An-Najah National University, Nablus, Palestine. E-mail: naim.kittana@najah.edu*
[c]*Department of Chemistry, Faculty of Sciences, An-Najah National University, Nablus, Palestine*

© 2023 The Author(s). Published by the Royal Society of Chemistry

Open Access Article. Published on 02 March 2023. Downloaded on 1/31/2025 1:53:19 PM.
This article is licensed under a Creative Commons Attribution-NonCommercial 3.0 Unported Licence.

approach suffers from low stability. On the other hand, covalent functionalization provides higher water dispersibility and stability which involves the formation of covalent adducts with the sp^2 carbon structures in graphene.[16,17] One of the successful and effectively developed functionalization approaches is the electrophilic substitution of aryl diazonium salt on the surface of the graphene sheet which provides tremendous applications in various fields.[18–21] Herein, we used this method to covalently functionalize graphene sheets with adequate molecules of a hydrophilic linker (derived from tetraethylene glycol) to improve the water dispersibility of the graphene. In addition, to load plasmid DNA (pDNA), it is necessary to introduce tetramine spermine, which is a cationic linker on the surface of the graphene sheets. Tetramine spermine is a synthetic polyamine that showed efficient and safe gene delivery to the cells without the incidence of the immune response.[22–25] The resulting functionalized graphene (Scheme 1) was loaded with pDNA that encodes enhanced green fluorescence protein (eGFP) as a model to test its capacity to deliver genetic materials into cells. In this work, we aim to covalently functionalize the graphene sheets with the appropriate linkers to load the plasmid DNA and deliver the resulting complex to the cancer cells to achieve appropriate gene transfection. Moreover, the complexation of the functionalized graphene with the pDNA has been studied by quantum theoretical calculations.

2. Materials and methods

2.1. Reagents and instrumentation

All reagents were used as received without further purification. Propiolic acid, L-ascorbic acid sodium salt, anhydrous copper sulphate ($CuSO_4$), trifluoroacetic acid (TFA), 2-(1*H*-benzotriazole-1-yl)-1,1,3,3-tetramethylaminium tetrafluoroborate (TBTU), and tetraethylene glycol were purchased from Alfa Aesar Company, England. Graphene nano-powder was purchased from Nanostructured & Amorphous Materials, Inc. (NanoAmor), USA. Sodium azide, 4-nitrobenzylamine hydrochloride, *N*,*N*-diisopropylethylamine (DIPEA), di-*t*-butyl dicarbonate (BOC_2O), isoamyl nitrite were purchased from Sigma-Aldrich Company, Germany. Column chromatography was used for purification steps. Thin layer chromatography was used to observe the reaction and was purchased from DC-Fertigfolien ALUGERAM®SIL G/UV_{254}, MACHEREY NAGEL Company, Germany. A centrifuge (Zentrifugen, Germany) and a sonicator (Digital Ultrasonic Cleaner) were used to dissolve and disperse the functionalized graphene. For the gel electrophoresis test, agarose powder, ethylenediaminetetraacetic acid (EDTA), trizma powder, and sodium dodecyl sulfate (SDS) were purchased from Sigma-Aldrich Company, Germany. Plasmid eGFP was gifted by Professor Nabieh Ayob, Haifa. For the biological test, phosphate-buffered saline, fetal bovine serum 10% medium FBS, trypsin–EDTA solution 1X, and RPMI medium were purchased from Sigma-Aldrich Company, Germany. A transmission electron microscope (TEM) (FEI Company, Netherlands) was used to analyse the size and morphology of the graphene sheets. Ultraviolet-visible data was recorded on a 7315 Spectrophotometer, Jenway, UK. Nuclear Magnetic Resonance spectra were obtained using Bruker Avance 500 spectrometer, (Switzerland). Thermogravimetric analysis (TGA) spectra were recorded by (STA 409 PC Luxx®, NETZSCH) under nitrogen (100 cc min^{-1}) with a heating rate of 20 °C min^{-1} in a range of 25–600 °C. Zeta potential was measured by NanoBrook Omni, Brookhaven Instruments Corporation, USA. A fluorescence microscope (Olympus) was used to detect the GFP protein.

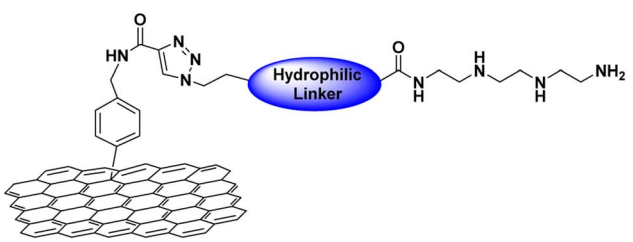

Scheme 1 The designed covalent functionalization of graphene sheets with tetramine linker.

2.2. Synthesis and characterization

All the synthetic procedures and gene experiments were prepared at An-Najah University laboratories. NMR, TEM, and TGA measurements were conducted at the University of Jordan.

2.2.1. Synthesis of triethylenetetramine-Boc (1). Triethylenetetramine (745 μl, 5 mmol) was added to dried methanol (70 ml) under vacuum and argon. Ethyl trifluoroacetate (595 μl, 5 mmol) was added dropwise for 45 minutes under controlled nitrogen (N_2) atmosphere at (−70 °C), the reaction was stirred for another 45 minutes, then the temperature was increased to 0 °C and was stirred 1 h. Di *tert*-butyl dicarbonate (4 g, 18.75 mmol) was dissolved in 10 ml dried methanol under argon and was added dropwise over 30 minutes at 0 °C. The reaction warmed to room temperature and stirred for 24 h. The reaction was extracted with dichloromethane (DCM) (50 ml) and washed with sodium bicarbonate ($NaHCO_3$) 10% and then with 40 ml distilled water. The organic layer was separated and dried over sodium sulphate (Na_2SO_4) and then evaporated. The product was recrystallized from DCM/methanol in refrigeration for 10 h to afford white powder crystals. The product was filtrated under a vacuum and the powder was dissolved in 70 ml of methanol then the potassium carbonate (0.58 g dissolved in water) was added to the powder solution and refluxed. The reaction was concentrated and purified by using silica gel column chromatography (DCM : MeOH : NH_4OH 10 : 1 : 0.1) to provide triethylenetetramine-Boc compound (**1**) (yield: 73%, 533.8 mg). R_f: 0.48 (DCM : MeOH : NH_4OH) (10 : 1 : 0.1). ^1H NMR (500 MHz, $CDCl_3$): δ 3.35–3.20 (bm, 10H, $4CH_2N$ & CH_2NH), 2.68 (bt, 2H, CH_2NH_2), 1.41 (s, 27H, $C(CH_3)_3$), 1.35 (s, 2H, NH_2).

2.2.2. Synthesis of OH-TEG-OTs (2), synthesis of OH-TEG-N_3 (3), and synthesis of COOH-TEG-N_3 (4). The synthesis and identification of these compounds as they reported in the literature.[26–28]

2.2.3. Synthesis of N_3-TEG-tetramine-Boc (5). COOH-TEG-N_3 (**4**) (165 mg, 0.71 mmol) and TBTU (295.1 mg, 0.78) were added to the flask under vacuum and argon. A solution of

Open Access Article. Published on 02 March 2023. Downloaded on 1/31/2025 1:53:19 PM. This article is licensed under a Creative Commons Attribution-NonCommercial 3.0 Unported Licence.

triethylenetetramine-Boc (**1**) (347.6 mg, 0.45 mmol), DIPEA (408 μl, 2.334 mmol) in acetonitrile (10 ml) was added to the mixture and was stirred at room temperature for 24 h. The reaction was extracted with DCM (60 ml) and HCl 1 M (30 ml) and was dried. The resulting was purified with the use of a mobile phase of (DCM : MeOH) (15 : 1) to obtain compound (**5**) as an oily product (yield 75.2%, 261.4 mg). FTIR: 3345 (NH), 2928 (CH_2), 2105 (N_3), 1688 (CO) cm^{-1}. ^{1}H NMR (500 MHz, $CDCl_3$): δ 3.96 (s, 2H, C$\underline{H}_2$CONH), 3.68–3.64 (m, 8H, 4CH_2O), 3.39–3.24 (m, 16H, 4CH_2N, 2CH_2NH, COC$\underline{H}_2$CH_2N_3 & COCH_2C$\underline{H}_2$O), 2.2 (t, 2H, J = 4.4 Hz, CH_2N_3), 1.44 (s, 27H, C(CH_3)$_3$).

2.2.4. Synthesis of *N*-(4-nitrobenzyl) propiolamide (6). Propiolic acid (211 μl, 2.92 mmol), TBTU (1.11 g, 1.17 mmol), and *p*-nitrobenzyl amine (500 mg, 2.65 mmol) were mixed in a flask under argon, after that DIPEA (1.39 ml, 7.92 mmol) and acetonitrile (15 ml) were added to the flask and stirred overnight. Then the product was extracted with DCM (60 ml) and was washed with HCl 1 M (30 ml) and dried. Then the reaction passes the purification step with a mobile phase of Hex : EtOAc (1 : 2) to obtain the product as a yellowish powder. The yield was (339 mg, 67%). ^{1}H NMR (500 MHz, $CDCl_3$): δ 8.20 (d, 2H, J = 4.9 Hz, Ph), 7.44 (d, 2H, J = 4.8 Hz, Ph), 6.42 (bs, 1H, NH), 4.57 (d, 2H, J = 5.9 Hz, C$\underline{H}_2$NH), 2.84 (s, 1H, C≡CH). ^{13}C NMR (125.7 MHz, $CDCl_3$): δ 159.0, 152.3, 147.6, 128.4, 124.1, 75.4, 74.4, 43.1.

2.2.5. Synthesis of *N*-(4-aminobenzyl) propiolamide (7). Compound 6 (339 mg, 1.66 mmol) dissolved in a mixture of methanol : H_2O (2 : 1), then zinc powder (977 mg, 14.9 mmol) and ammonium chloride (194.2 mg, 3.63 mmol) were added to the reaction and stirred under reflux for 4 h. The reaction was filtrated then washed with ethyl acetate then evaporated to yield a yellowish product with a yield of 300 mg, 88.5%. R_f: 0.70 (Hex/EtOAc 1 : 2). ^{1}H NMR (500 MHz, $CDCl_3$): δ 7.28 (t, 1H, J = 7.8 Hz, NHCO), 7.08 (d, 2H, J = 8.8 Hz, Ph), 6.64 (d, 2H, J = 8.5 Hz, Ph), 5.63 (s, 2H, NH_2), 4.38 (d, 2H, J = 5.6 Hz, C$\underline{H}_2$NH), 3.72 (s, 1H, C≡CH). ^{13}C NMR (125.7 MHz, $CDCl_3$): δ 148.4, 145.2, 130.9, 129.3, 129.0, 115.3, 73.2, 72.2, 43.4.

2.2.6. Synthesis of graphene–alkyne (8). Compound 7 (150 mg, 0.861 mmol) was mixed with graphene (45 mg) powder and dried under vacuum and argon. 1,2-Dichlorobenzene (ODCB) (13 ml) dissolved in 10 ml acetonitrile was added, then sonicated for 10 minutes. Iso-amyl nitrite (693.8 μl, 5.166 mmol) was added gradually and stirred for 24 h at 60 °C. After that, a centrifugation step was done for 15 minutes then the product was washed with MeOH (2 × 30 ml), DCM (2 × 30 ml), and Et_2O (2 × 30 ml). The product was collected with diethyl ether and dried to yield compound (**8**) (50 mg).

2.2.7. Click reaction of graphene–alkyne with N_3-TEG-tetramine-Boc (9). Ascorbic acid (13.5 mg, 198.1 mmol) and anhydrous copper sulphate (3.6 mg, 0.022 mmol) were dissolved in distilled H_2O (4 ml) and the solution was added to a sonicated solution of the N_3-TEG-tetramine-Boc (**5**) (100 mg, 0.15 mmol) and graphene–alkyne (**8**) (25 mg) dissolved in DCM (4 ml). The reaction was stirred for 24 h. After that, MeOH (20 ml) was added and sonicated followed by centrifugation for 15 min and the supernatant was discarded and washing steps were conducted with MeOH (2 × 20 ml) and Et_2O (2 × 15 ml) then collected with diethyl ether. The resulting compound was (30 mg).

2.2.8. Deprotection of Boc groups (10). Functionalized graphene (**9**) (33 mg) was dispersed in DCM (4 ml). Then, trifluoroacetic acid (4 ml) was added and stirred for 24 h. After that, MeOH (20 ml) was added to the resulting product and then sonicated and centrifuged for 10 min washing steps were repeated by using MeOH (2 × 15 ml), DCM (15 ml) then distilled water, and diethyl ether (2 × 15 ml). The obtained weight of the powder was 29 mg.

2.2.9. Kaiser test protocol to determine the free NH_2 loading. The experiment was done according to the literature and the result was expressed as μmole of amino groups per gram of functionalized graphene. (1.1 mg) of functionalized graphene (**10**) was weighted in a small tube. Phenol solution (75 μl), pyridine solution (100 μl), and ninhydrin solution (75 μl) were added to the tube. The blank was prepared exactly with the same quantities of solvents but without the functionalized graphene. The resulting dispersion was sonicated for 5 min and was heated for 10 minutes at 120 °C. The suspension was cooled and diluted with 60% ethanol (1 ml) and filtered by a glass dropper. The tube was washed with 60% ethanol (2 × 0.5 ml). After that, the filtrate was analysed by UV spectroscopy at 570 nm.

2.2.10. Transmission electron microscope analysis. An aliquot of the functionalized graphene (**10**) was dropped on a carbon-coated grid, then left to be dried, and then analysed by the TEM apparatus.

2.2.11. Zeta-potential measurement. 1% concentration of the functionalized graphene (**10**) was sonicated for 10 min at room temp and zeta potential was measured by Brookhaven instrument.

2.3. Complexion of f-graphene (10) with pEGFP-c1

f-Graphene was mixed with the plasmid DNA (pDNA) pEGFP-C1 at different N/P ratios; 5 : 1, 7.5 : 1, and 10 : 1 (N/P ratio defined as the molar ratio of nitrogen in f-graphene to phosphate group in the DNA (N/P ratio)). To guarantee the consistency of the signal intensity on the gel, the amount of the pDNA was fixed while the amount of f-graphene was increased according to the intended N/P ratio. The mixtures of f-graphene and pDNA were mixed vigorously and then were then incubation for 45 min at 37 °C. Equal volumes of each sample were loaded per well of 0.8% agarose gel submerged in TAE buffer. The electrophoresis was run at a voltage of 110 volts for 30 min. The gel was visualized by a UV PhotoDoc-It imaging system.

2.4. Plasmid DNA release assay

An efficient release of pDNA from the pDNA–f-graphene is essential for the successful expression of the transfected genes.[29] Therefore as a model, this possibility was investigated by using the nonionic surfactant sodium dodecyl sulfate (SDS) aqueous solution at a concentration that was added to the pDNA–graphene complex.[30] Afterward, the samples were subjected to agarose gel electrophoresis.

 © 2023 The Author(s). Published by the Royal Society of Chemistry

Open Access Article. Published on 02 March 2023. Downloaded on 1/31/2025 1:53:19 PM.
This article is licensed under a Creative Commons Attribution-NonCommercial 3.0 Unported Licence.

2.5. *In vitro* plasmid pEGFP-C1 transfection experiment

For *in vitro* transfection experiments, HeLa cells were cultured in RPMI medium at standard laboratory conditions at a density of 6×10^4 cells per well of 48-well plates. The complex pDNA–f-graphene, which was prepared as a 10 : 1 ratio (containing a total of 3 μg pDNA), was added per well, and the culture plates were incubated for 24 h, then 250 μl of fresh RPMI containing 6.2 μl of 0.01% Tween was added. In parallel, a control experiment was done in wells without cells to rule out the autofluorescence of the test compound. After that, the HeLa cells were examined by fluorescence microscopy to check for the expression of the enhanced green fluorescent protein (eGFP).

2.6. Cell viability test

The cells were seeded in a plastic plate (96 well) in a density of 5×10^3 per well overnight then the cells were incubated for 3 h with the f-graphene at a concentration equivalent to that used in the transfection experiment (4.32 mg ml^{-1}). After that, 3-(4,5-dimethylthiazol-2-yl)-5-(3-carboxymethoxyphenyl)-2-(4-sulfophenyl)-2*H*-tetrazolium (MTS) solution was added to each well and the plate was incubated for 4 h in the cell culture incubator and the absorbance was measured at a wavelength of 490 nm.

2.7. Theoretical calculations

To investigate the bonding interactions involved in this work, the graphene sheets were first optimized using the BAND engine in Amsterdam Modelling Suite (AMS) 2022.[31,32] Starting from the reported graphene's structure, a single sheet of 11 × 11 rings was constructed, and optimized, allowing the optimization along the *XY*-plane under periodic boundary conditions. The optimization was done using the Perdew–Burke–Ernzerhof (PBE) exchange-correlation functional with Grimme's dispersion (PBE-D),[33,34] and the double-ζ basis set (DZP). This level of theory has demonstrated good performance in similar previous studies.[35–38] Scalar relativistic effects were treated with the ZORA approach,[39–41] and a large frozen core. All geometry optimizations were completed with an energy cut-off of 0.0001 Ha, and a gradient convergence of 0.005 Ha $Å^{-1}$. In the next step, the linker functional group (*cf.* Scheme 1) was attached to the graphene surface, and its interaction with a simplified DNA sequence was studied under the same level of theory. During this geometry optimization, the coordinates of the graphene surface atoms were constrained while all other atoms were relaxed.

The binding energy between the f-graphene/linker and the DNA functional groups was calculated by:

$$\Delta H_{298}\,(\text{reaction}) = \Delta H_{298}\,(\text{products}) + \Delta H_{298}\,(\text{reactants}) \quad (1)$$

where the enthalpy at 298 K for a given species is given by:

$$H_{298} = \text{SPE} + \text{ZPE} + H_{\text{corr.}} \quad (2)$$

where SPE is the single-point energy, ZPE is the zero-point energy, and $H_{\text{corr.}}$ is the enthalpy correction at 298 K.

Finally, the quantum theory of atoms in molecules (QTAIM) calculations were done on the optimized system from the previous step, using the ADF engine in AMS.[42,43] The criteria for determining the type of electrostatic interactions from the QTAIM calculations were based on previous publications.[44] Further details on the calculations can be found in previous studies.[37,45,46]

3. Results and discussion

3.1. Synthesis and functionalization of graphene sheets

The synthesis of the functionalized graphene was achieved in multi-steps. Beginning with the synthesis of the tetramine-Boc linker (**1**) that was connected to another linker (**4**) derived from tetraethylene glycol to improve the water dispersibility of the graphene sheets and to form a complex with the plasmid DNA through electrostatic interaction. So, the synthesis of tetramine-Boc (**1**) was achieved by selective protection of one of the primary amine groups of the triethylenetetramine by ethyl trifluoroacetate at −78 °C, followed by the protection of the other amine groups by the addition of di *tert*-butyl dicarbonate (Boc_2O) to obtain the fully protected amine groups. After that, the trifluoroacetyl group was cleaved at basic pH using potassium carbonate then recrystallization of the product to obtain the pure triethylenetetramine-Boc (**1**). The second linker (**4**) was synthesized starting from tetraethylene glycol (TEG) by converting one of the hydroxyl groups to tosyl to obtain the OH-TEG-OTs (**2**). Then, the tosyl group was reacted with sodium azide in ethanol to obtain the OH-TEG-N_3 (**3**). Finally, compound (**3**) was oxidized by Jone's reagent to obtain the required linker (**4**). After that, the tetramine-Boc (**1**) was connected with linker (**4**) through an amidation reaction using TBTU as a coupling agent and DIPEA as a base to obtain compound (**5**), as shown in Scheme 2.

The bonding between the synthesized N_3-TEG-tetramine-Boc (**5**) and the graphene sheets was achieved through a click reaction, which is a copper-catalyzed azide–alkyne cycloaddition reaction to form a triazole ring. This reaction is facile and rapid with a high yield that was discovered by Fokin, Sharpless, and Meldal.[47–49] As the azide linker was successfully synthesized, the alkyne group needs to be attached to the graphene sheet. *N*-(4-Nitrobenzyl)propiolamide (**6**) was prepared by the formation of an amide linkage between *p*-nitrobenzyl amine

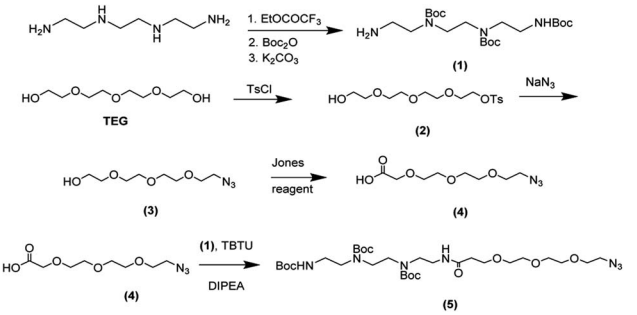

Scheme 2 Synthesis of N_3-TEG-tetramine-Boc (**5**).

Open Access Article. Published on 02 March 2023. Downloaded on 1/31/2025 1:53:19 PM.
This article is licensed under a Creative Commons Attribution-NonCommercial 3.0 Unported Licence.

and propiolic acid using TBTU and DIPEA to get compound (**6**) followed by the reduction of the nitro group to amine group using zinc and ammonium chloride in presence of 10% MeOH to produce compound (7). The covalent functionalization of graphene sheets was carried out through electrophilic aromatic substitution using diazonium salt.[50] Therefore, the amine group of compound (7) was reacted with isoamyl nitrite to form the diazonium salt in the presence of *o*-DCB, and acetonitrile as solvents. Followed by the addition of graphene sheets to get the functionalized graphene (**8**) terminated with the alkyne group as shown in Scheme 3.

After the synthesis of graphene–alkyne (**8**). It was effectively bonded with compound (**5**) through a click reaction. In this experiment, a click reaction was employed by using anhydrous $CuSO_4$ and ascorbic acid as catalysts, which dissolved in distilled H_2O and DCM to obtain f-graphene (**9**). In a final step, a deprotection reaction was conducted to obtain free amine groups in the presence of trifluoroacetic acid (TFA) in DCM to obtain the required graphene-TEG-tetramine (**10**) as shown in Scheme 4. To determine the amount of free amine loaded on the surface of graphene sheets, the Kaiser test was conducted to obtain a total amine-loaded amount of 0.135 mmol per gram of graphene which confirms the successful functionalization of the graphene sheets with the tetraamine linker.

3.2. Characterization of functionalized graphene

3.2.1. Dispersibility, morphology, and zeta potential analysis of the functionalized graphene. Pristine graphene is considered hydrophobic in nature and showed low water dispersibility and rapid precipitation in water due to the van der Waals interactions between the sheets as observed in Fig. 1(A, I). The TEM analysis showed the formation of aggregated graphene sheets due to the hydrophobic interaction between them as shown in Fig. 1(A, II). However, upon the functionalization of the graphene sheets with the hydrophilic groups, they became dispersed in water with good stability as shown in Fig. 1(B, I). Moreover, the TEM image of the f-graphene (**10**) demonstrates the separation of the graphene sheets as can be observed in Fig. 1(B-II).

Moreover, zeta potential measurement was used to determine the net charge on the surface of the nanomaterials and provide additional information on the physical stability of the formed suspension.[51,52] Therefore, the zeta potential obtained for the functionalized graphene was +29 mV, which indicates a positive charge surrounding the surface of the graphene sheet due to the tetramine functionalization. This positive charge will increase the stability due to the repulsion effect and prevent the aggregation and precipitation behavior of the pristine graphene.

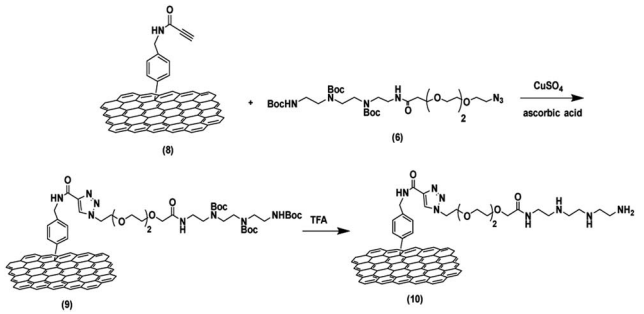

Scheme 4 The functionalization and synthesis of graphene-TEG-tetramine (**10**).

3.2.2. Thermogravimetric analysis (TGA). The graphene sheets are thermostable and do not degrade upon heating until 600 °C with minimum weight loss,[53,54] while most organic materials are decomposed at this high temperature. Therefore, thermogravimetric analysis was conducted to quantify the loaded amount of organic material on the surface of the graphene sheets. TGA was performed under nitrogen for the pristine and f-graphene (**10**). The two samples were heated until 600 °C and the weight loss was recorded as a function of temperature.[55] As shown in Fig. 2, pristine graphene did not lose any weight due to its thermal stability. Therefore, the weight loss in the case of the f-graphene (**10**) will be corresponding to the amount of functionalization. As shown in Fig. 2 the percentage of weight loss was 58% of the f-graphene which will correspond to the amount of functionalization which indicates a high functionalization of the graphene.

3.3. Evaluation of graphene–pDNA complex formation and dissociation

Agarose gel electrophoresis was employed to investigate the formation of pDNA–f-graphene complex at various N/P ratios (5 : 1, 7.5 : 1, and 10 : 1). This would be indicated by a retard of pDNA migration through an agarose gel. At the same time, pDNA–f-graphene complex formation should be reversible as the pDNA should be released inside the cells to be available for

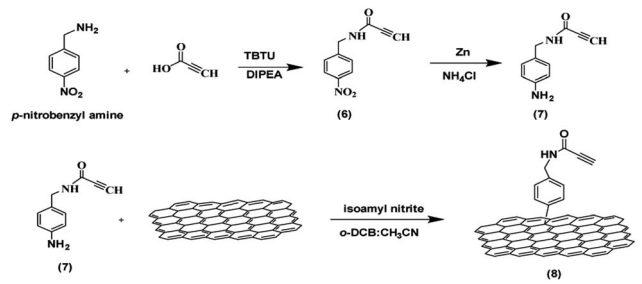

Scheme 3 Synthesis of graphene alkyne (**8**).

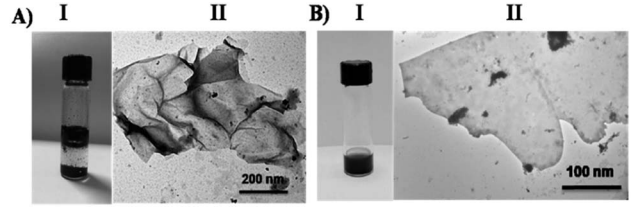

Fig. 1 (A) (I) A vial of pristine graphene mixed with water; (II) TEM image of pristine graphene. (B) (I) A vial of f-graphene (**10**); (II) TEM image of f-graphene (**10**).

© 2023 The Author(s). Published by the Royal Society of Chemistry

Open Access Article. Published on 02 March 2023. Downloaded on 1/31/2025 1:53:19 PM.
This article is licensed under a Creative Commons Attribution-NonCommercial 3.0 Unported Licence.

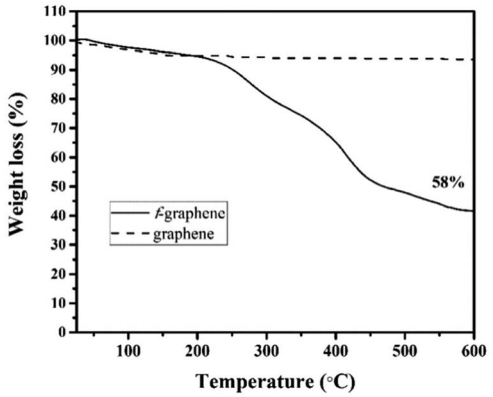

Fig. 2 TGA of pristine graphene (dashed line), f-graphene (10) (solid line).

the expression of the molecular machinery of the cells. To investigate this capability, the pDNA–f-graphene complex was incubated with SDS anionic surfactant that is expected to dissociate pDNA from graphene. As shown in Fig. 3, compared to the others, the N/P ratio of 10 : 1 completely inhibited pDNA migration. At the same time whenever pDNA–f-graphene complex was pre-incubated with SDS, a pDNA band was observed on the agarose gel. Taken together, the use of the 10 : 1 N/P ratio could result in a successful formation of a reversible complex. The formation of this complex is supported by the findings of the theoretical calculations, as discussed later in section 3.6.

3.4. Transfection of HeLa cells with pDNA–f-graphene complex

To evaluate the potential for the expression of genes carried by pDNA *in vitro*, HeLa cells were incubated with the pDNA–f-graphene complex prepared at the 10 : 1 N/P ratio. The used pDNA contains a reporter gene encoding for enhanced green fluorescent protein (EGFP), which is traditionally used to evaluate the efficiency of transfection.[56] The transfection was evaluated by fluorescence microscopy after incubating the cells with the test compounds for 1 h. Cell culture wells containing pDNA–f-graphene without cells were also imaged to rule out auto-fluorescence (negative control). As shown in the lower panel of Fig. 4, a green signal was observed in many of the cells incubated with pDNA–f-graphene complex, something that was not observed in the absence of cells (upper panel), which indicates a successful transfection of the pDNA in the HeLa cells, and a successful expression of the carried-on genes. More details on the exact interaction between the pDNA and the graphene complex are to be discussed in section 3.6.

3.5. Cell viability assay

Pristine carbon nanoparticles were reported in the literature to be cytotoxic for different types of cells.[57] Therefore, it was necessary to test whether this risk could be reduced by the implemented functionalization and the respective increase in hydrophilicity. The toxicity of f-graphene at an N/P ratio of 10 : 1 was investigated by using the MTS test on HeLa cells, as shown in Fig. 5. Using similar transfection conditions as in the experiments described above, there was no change in the percentage of cell viability between the control cells and those incubated with f-graphene, which indicates no cytotoxicity for f-graphene under these conditions.

3.6. Bonding interactions based on theoretical calculations

In the previous sections, we showed that the graphene/tetramine linker was bound strongly with pDNA through electrostatic interaction. To better understand this interaction, we studied a molecular system made of the tetramine linker bonded to a graphene sheet, and two nucleobases (guanine–thymine) that resemble the pDNA. The theoretical study was done as described in the experimental section (2.7).

First, the tetramine linker/graphene structure was optimized under periodic boundary conditions, as shown in Fig. 6. This serves as a benchmark before adding the unit resembling the pDNA. Next, the optimization was repeated by placing the G–T

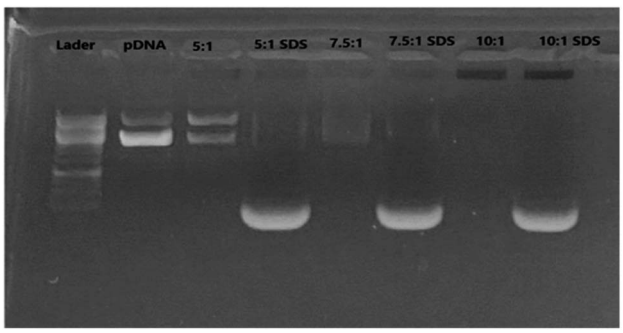

Fig. 3 Agarose gel electrophoresis subjected to UV light to visualize DNA bands. The migration of pDNA was retarded to variable degrees at different N/P ratios (5 : 1, 7.5 : 1, and 10 : 1). The addition of SDS resulted in the release of pDNA from the f-graphene and therefore the re-appearance of the pDNA bands in the gel.

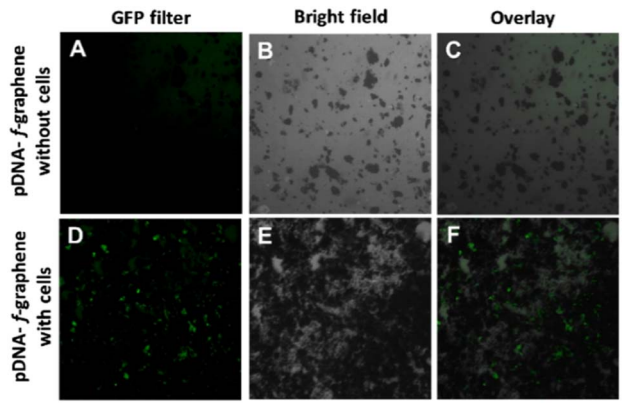

Fig. 4 The detection of EGFP fluorescent signal in HeLa cells after incubation with a pDNA–f-graphene complex. The first column shows sample imaging by using the GFP fluorescence filter. The second column is the bright field imaging and the third column is the overlay of both images. The images were processed by ImageJ® software.

Open Access Article. Published on 02 March 2023. Downloaded on 1/31/2025 1:53:19 PM.
This article is licensed under a Creative Commons Attribution-NonCommercial 3.0 Unported Licence.

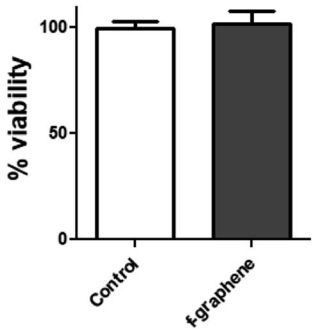

Fig. 5 Investigation of the effect of f-graphene on the viability of HeLa cells by using the MTS test, Student's *t*-test was used to compare the means, $\alpha = 0.05$, $n = 5$.

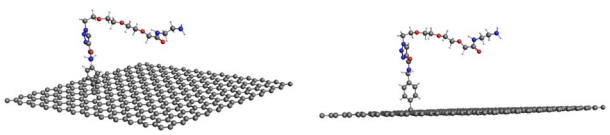

Fig. 6 Two different views for the optimized structure of graphene/tetramine linker as obtained at PBE-D/DZP level of theory.

base pair next to the linker. The optimization was done in two stages, with the G–T pair placed on opposite sides of the linker; the ether (a) and amine (b) parts, as shown in Fig. 7. The geometry of the entire system reflects that the G–T pair is well aligned along either side of the tetramine linker, as originally hypothesized in this work. Furthermore, it appears that strong interaction exists between the G–T base and the linker, due to the close bond distances between the two. For instance, the OH···O bond distance between the linker and the base is 1.32 Å in Fig. 7a, and 1.57 Å in Fig. 7b. This strongly suggests the formation of hydrogen bonding between the two moieties. The binding energy between the linker and the G–T base pair was calculated using eqn (1) in the theoretical section in terms of standard enthalpy change at 298 K (ΔH_{298}). The value was discovered to be 74.9 kJ mol^{-1}, which occurs within the scale of intermolecular attractions.

To further confirm this type of interaction, we performed QTAIM calculations on the optimized structure as previously described in the theoretical section (2.7). The QTAIM theory, also known as Bader's theory, locates critical points (CP) in molecular structures by using the topology of the electron density (ρ) and its Laplacian ($\nabla^2\rho$) structures.[44,58] For each CP, the calculations produce other parameters, such as the local potential energy density (V(b)), local gradient kinetic energy density (G(b)), and total energy density (H(b)), that can be used to reveal the nature of bonding between two atoms. The strength of QTAIM lies in its description of the CP's located between molecules–known as bond critical points (BCP). The latter can be classified as either a shared interaction (*e.g.*, covalent and polar) or a closed-shell interaction (*e.g.*, hydrogen bond, ionic, van der Waals).

Fig. 8 depicts the QTAIM topology of the tetramine linker/G-T base at the PBE-D/DZP level of theory. The linker is aligned along the ether side (Fig. 8a) and the amine side (Fig. 8b). The QTAIM parameters for the two geometers, *a* and *b*, are also listed in Table 1. All the BCP in the table are characterized with a rank and signature of (3, −1), indicating an intermolecular interaction. The electron densities are on the scale of 0.01 to 0.1 Hartree, which is a typical range for intermolecular bonding (covalent bonds have higher values). All Laplacian values in Table 1 are positive and in the range of 10^{-2} Harreee, indicating van der Waals interaction.[44,58]

One particular BCP, #4, has a higher Laplacian value of 0.083 Harreee. This BCP corresponds to the OH···H bond between the linker and the G–T base pair as shown in Fig. 8a. A useful criterion for identifying the nature of a BCP is the ratio of potential (V) and kinetic energy (G) densities. If the ratio is less than one, the bond is considered a pure closed shell (*i.e.*, ionic, H-bonding, VDV). Otherwise, the bond is considered a regularly closed shell (*i.e.* covalent). In the case of BCP #4, the V/G ratio is 1.8, and the bond energy, on the other hand, can be considered as half the value of Vb.[59] Table 1 shows a value of 228.4. The V/G ratio and relatively high bond energy value of BCP #4 highly suggest that it is a strong VDV bond.

A similar observation can be observed from Table 1 for BCP #5. The Laplacian, bond energy, and V/G ratio for this point are 0.181 H, 92.1 kJ mol^{-1}, and 1.2, respectively. These parameters suggest it is a strong H-bond, based on the above criteria.

Thus, there are 17 BCPs between the tetramine linker and the G–T base, with two of them referring to strong bonding. This finding is in concert with the experimental results described in this work.

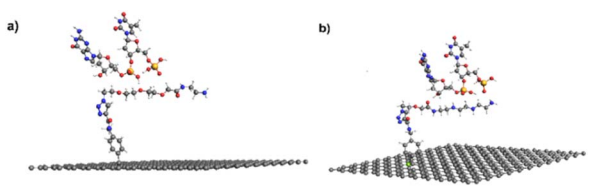

Fig. 7 Two optimized structures of the graphene/tetramine linker with the guanine-thymine nucleobases. (a) From the ether side, and (b) from the amine side. Obtained at the PBE-D/DZP level of theory.

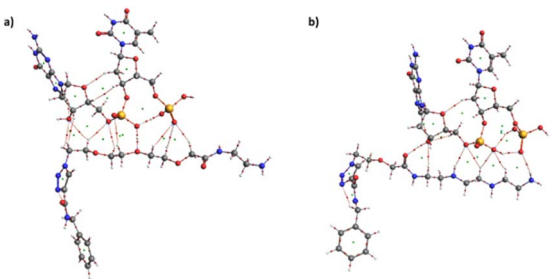

Fig. 8 Schematic representation of the electron density superimposed on the Laplacian contour maps of the graphene/tetramine linker with the guanine-thymine nucleobases. (a) From the ether side, and (b) from the amine side. Obtained at PBE-D/DZP level of theory. Red dots = BCP, green dots = ring CP.

© 2023 The Author(s). Published by the Royal Society of Chemistry

Open Access Article. Published on 02 March 2023. Downloaded on 1/31/2025 1:53:19 PM.
This article is licensed under a Creative Commons Attribution-NonCommercial 3.0 Unported Licence.

Table 1 BCP topological properties for geometry-*a* and *b*, as obtained from QTAIM calculations at B97-D/DZP level of theory

CP #	1	2	3	4	5	6	7	8	9	10
Geometry *a*										
Rho	0.018	0.008	0.005	0.120	0.008	0.010	0.011	0.008	0.006	0.008
Laplacian	0.070	0.028	0.020	0.083	0.028	0.039	0.044	0.032	0.025	0.031
Gb	0.015	0.006	0.004	0.097	0.006	0.008	0.009	0.006	0.005	0.006
Vb	−0.013	−0.004	−0.003	−0.174	−0.004	−0.006	−0.007	−0.005	−0.003	−0.004
Hb	0.002	0.001	0.001	−0.077	0.001	0.002	0.002	0.002	0.001	0.002
$\frac{1}{2}V$(b) (kJ mol^{-1})	17.4	5.4	3.4	228.4	5.4	7.7	9.2	6.0	4.4	5.8
V/*G*	0.9	0.7	0.7	1.8	0.7	0.8	0.8	0.7	0.7	0.7

CP #	1	2	3	4	5	6	7
Geometry *b*							
Rho	0.011	0.009	0.012	0.006	0.061	0.013	0.010
Laplacian	0.044	0.038	0.047	0.024	0.181	0.048	0.038
Gb	0.009	0.008	0.010	0.005	0.058	0.010	0.008
Vb	−0.007	−0.006	−0.008	−0.003	−0.070	−0.008	−0.006
Hb	0.002	0.002	0.002	0.001	−0.012	0.002	0.002
$\frac{1}{2}$ *V*(b) (kJ mol^{-1})	8.6	7.3	10.1	4.2	92.1	10.7	7.4
V/*G*	0.8	0.7	0.8	0.7	1.2	0.8	0.7

4. Conclusions

Graphene sheets were covalently functionalized with the appropriate linkers to improve their water dispersibility and to provide a positive charge on their surface. The TEM image of the f-graphene (**10**) confirms the functionalization and the separation of the graphene sheets with a degree of functionalization of 58% as obtained by TGA. Moreover, the zeta potential showed a value of +29 mV which indicates good water dispersibility with the decoration of the positive charge on the surface of the graphene sheet. Agarose gel electrophoresis with and without SDS demonstrated a successful formation of a reversible complex of pDNA with f-graphene, with an optimum N/P ratio of 10 : 1. *In vitro* studies demonstrated the capacity of this system to deliver DNA materials into cells, as illustrated by the detection of EGFP signal in HeLa cells treated with pDNA–graphene complex comparing with control. This was achieved without affecting the viability of the cells. In addition, quantum theoretical calculations suggested a strong binding between the pDNA, represented by a G-T base pair, and the functionalized graphene. The binding energy, in terms of enthalpy change (ΔH_{298}), was determined to be 74.9 kJ mol^{-1}. QTAIM calculations were used to further investigate the interactions, which revealed strong VDV and H-bond interactions. The development of f-graphene for gene delivery systems has great potential to establish a new family of drugs that might improve the treatment of many difficult diseases such as cancer and different types of genetic disorders.

Author contributions

The authors confirm their contribution to the paper as follows: study conception and design: M. Assali, N. Kittana. Theoretical calculations and modelling: I. Badran; perform the experiments: S. Omari; data analysis and validation, M. Assali, N. Kittana and I. Badran. Draft manuscript preparation: M. Assali, N. Kittana, and I. Badran. All authors reviewed the results and approved the final version of the manuscript.

Conflicts of interest

There are no conflicts to declare.

Acknowledgements

The authors thank the Association of Arab Universities for the fund. S. Omari thanks the Faculty of Graduate Studies at An-Najah National University to facilitate the achievement of this work.[61] The authors acknowledge Mrs. Duaa Qattan for TEM analysis and Hamdi Mango center for TGA analysis.

Notes and references

1 J. Reiser, X.-Y. Zhang, C. S. Hemenway, D. Mondal, L. Pradhan and V. F. La Russa, *Expert Opin. Biol. Ther.*, 2005, **5**, 1571–1584.
2 D. K. Chellappan, N. S. Sivam, K. X. Teoh, W. P. Leong, T. Z. Fui, K. Chooi, N. Khoo, F. J. Yi, J. Chellian and L. L. Cheng, *Biomed. Pharmacother.*, 2018, **108**, 1188–1200.
3 M. Vincent, I. de Lázaro and K. Kostarelos, *Gene Ther.*, 2017, **24**, 123.
4 J. T. Bulcha, Y. Wang, H. Ma, P. W. L. Tai and G. Gao, *Signal Transduction Targeted Ther.*, 2021, **6**, 53.
5 P. R. Riley and R. J. Narayan, *Curr. Opin. Biomed. Eng.*, 2021, **17**, 100262.

Open Access Article. Published on 02 March 2023. Downloaded on 1/31/2025 1:53:19 PM. This article is licensed under a Creative Commons Attribution-NonCommercial 3.0 Unported Licence.

6 I. Badran and M. O. Al-Ejli, *ChemistrySelect*, 2022, **7**, e202202976.
7 I. W. Almanassra, A. D. Manasrah, U. A. Al-Mubaiyedh, T. Al-Ansari, Z. O. Malaibari and M. A. Atieh, *J. Mol. Liq.*, 2020, **304**, 111025.
8 D. G. Papageorgiou, I. A. Kinloch and R. J. Young, *Prog. Mater. Sci.*, 2017, **90**, 75–127.
9 J. Shi and Y. Fang, in *Graphene*, Elsevier, 2018, pp. 215–232.
10 R. K. Layek and A. K. Nandi, *Polymer*, 2013, **54**, 5087–5103.
11 A. Lopez and J. Liu, *Advanced Intelligent Systems*, 2020, **2**, 2000123.
12 W. Yu, L. Sisi, Y. Haiyan and L. Jie, *RSC Adv.*, 2020, **10**, 15328–15345.
13 G.-h. Yang, D.-d. Bao, H. Liu, D.-q. Zhang, N. Wang and H.-t. Li, *J. Inorg. Organomet. Polym. Mater.*, 2017, **27**, 1129–1141.
14 V. Georgakilas, J. N. Tiwari, K. C. Kemp, J. A. Perman, A. B. Bourlinos, K. S. Kim and R. Zboril, *Chem. Rev.*, 2016, **116**, 5464–5519.
15 J. A. Mann and W. R. Dichtel, *J. Phys. Chem. Lett.*, 2013, **4**, 2649–2657.
16 C. Wetzl, A. Silvestri, M. Garrido, H. L. Hou, A. Criado and M. Prato, *Angew. Chem., Int. Ed.*, 2022, e202212857.
17 J. Sturala, J. Luxa, M. Pumera and Z. Sofer, *Chem.–Eur. J.*, 2018, **24**, 5992–6006.
18 J. R. Lomeda, C. D. Doyle, D. V. Kosynkin, W.-F. Hwang and J. M. Tour, *J. Am. Chem. Soc.*, 2008, **130**, 16201–16206.
19 A. Sinitskii, A. Dimiev, D. A. Corley, A. A. Fursina, D. V. Kosynkin and J. M. Tour, *ACS Nano*, 2010, **4**, 1949–1954.
20 H. Zhang, E. Bekyarova, J.-W. Huang, Z. Zhao, W. Bao, F. Wang, R. C. Haddon and C. N. Lau, *Nano Lett.*, 2011, **11**, 4047–4051.
21 M. Assali, M. Almasri, N. Kittana and D. Alsouqi, *ACS Biomater. Sci. Eng.*, 2019, **6**, 112–121.
22 T. Dewa, T. Asai, Y. Tsunoda, K. Kato, D. Baba, M. Uchida, A. Sumino, K. Niwata, T. Umemoto, K. Iida, N. Oku and M. Nango, *Bioconjugate Chem.*, 2010, **21**, 844–852.
23 P. A. Puchkov and M. A. Maslov, *Pharmaceutics*, 2021, **13**, 920.
24 P. A. Puchkov, K. A. Perevoshchikova, I. A. Kartashova, A. S. Luneva, T. O. Kabilova, N. G. Morozova, M. A. Zenkova and M. A. Maslov, *Russ. J. Bioorg. Chem.*, 2017, **43**, 561–569.
25 H. M. Ghonaim, S. Li and I. S. Blagbrough, *Pharm. Res.*, 2009, **27**, 17–29.
26 M. Assali, A. N. Zaid, N. Kittana, D. Hamad and J. Amer, *Nanotechnology*, 2018, **29**, 245101.
27 M. Assali, N. Kittana, S. Alhaj-Qasem, M. Hajjyahya, H. Abu-Rass, W. Alshaer and R. Al-Buqain, *Sci. Rep.*, 2022, **12**, 12062.
28 M. Assali, N. Kittana, S. Dayyeh and N. Khiar, *Nanotechnology*, 2021, **32**, 205101.
29 S. R. Dave and X. Gao, *Wiley Interdiscip. Rev.: Nanomed. Nanobiotechnol.*, 2009, **1**, 583–609.
30 J. M. Benns, J.-S. Choi, R. I. Mahato, J.-S. Park and S. W. Kim, *Bioconjugate Chem.*, 2000, **11**, 637–645.
31 G. te Velde, F. M. Bickelhaupt, E. J. Baerends, C. Fonseca Guerra, S. J. A. van Gisbergen, J. G. Snijders and T. Ziegler, *J. Comput. Chem.*, 2001, **22**, 931–967.
32 P. H. T. Philipsen, G. te Velde, E. J. Baerends, J. A. Berger, P. L. de Boeij, M. Franchini, J. A. Groeneveld, E. S. Kadantsev, R. Klooster, F. Kootstra, M. C. W. M. Pols, P. Romaniello, M. Raupach, D. G. Skachkov, J. G. Snijders, C. J. O. Verzijl, J. A. Celis Gil, J. M. Thijssen, G. Wiesenekker, C. A. Peeples, G. Schreckenbach and T. Ziegler, *BAND 2022.1, SCM, Theoretical Chemistry*, Vrije Universiteit, Amsterdam, The Netherlands, **http://www.scm.com**.
33 S. Grimme, S. Ehrlich and L. Goerigk, *J. Comput. Chem.*, 2011, **32**, 1456–1465.
34 J. P. Perdew and Y. Wang, *Phys. Rev. B*, 2018, **98**, 079904.
35 J. Sun, A. Ruzsinszky and J. P. Perdew, *Phys. Rev. Lett.*, 2015, **115**, 036402.
36 I. V. Lebedeva, A. V. Lebedev, A. M. Popov and A. A. Knizhnik, *Comput. Mater. Sci.*, 2017, **128**, 45–58.
37 I. Badran, N. S. Riyaz, A. M. Shraim and N. N. Nassar, *Comput. Theor. Chem.*, 2022, **1211**, 113689.
38 A. Förster and L. Visscher, *J. Chem. Theory Comput.*, 2021, **17**, 5080–5097.
39 E. v. Lenthe, E. J. Baerends and J. G. Snijders, *J. Chem. Phys.*, 1993, **99**, 4597–4610.
40 E. v. Lenthe, E. J. Baerends and J. G. Snijders, *J. Chem. Phys.*, 1994, **101**, 9783–9792.
41 E. v. Lenthe, A. Ehlers and E.-J. Baerends, *J. Chem. Phys.*, 1999, **110**, 8943–8953.
42 J. I. Rodríguez, R. F. W. Bader, P. W. Ayers, C. Michel, A. W. Götz and C. Bo, *Chem. Phys. Lett.*, 2009, **472**, 149–152.
43 J. I. Rodríguez, *J. Comput. Chem.*, 2013, **34**, 681–686.
44 P. L. A. Popelier and P. Popelier, *Atoms in Molecules: An Introduction*, Prentice Hall, 2000.
45 I. Badran, A. Rauk and Y. Shi, *J. Phys. Chem. A*, 2019, **123**, 1749–1757.
46 I. Badran and Y. J. Shi, *J. Phys. Chem. A*, 2015, **119**, 590–600.
47 H. C. Kolb and K. B. Sharpless, *Drug Discovery Today*, 2003, **8**, 1128–1137.
48 C. W. Tornøe, C. Christensen and M. Meldal, *J. Org. Chem.*, 2002, **67**, 3057–3064.
49 V. V. Rostovtsev, L. G. Green, V. V. Fokin and K. B. Sharpless, *Angew. Chem., Int. Ed.*, 2002, **41**, 2596–2599.
50 C. D. Doyle and J. M. Tour, *Carbon*, 2009, **47**, 3215–3218.
51 S. Bhattacharjee, *J. Controlled Release*, 2016, **235**, 337–351.
52 M. Assali and N. Zohud, *Drug Dev. Res.*, 2020, **82**, 448–457.
53 F. Liu, M. Wang, Y. Chen and J. Gao, *J. Solid State Chem.*, 2019, **276**, 100–103.
54 H. Y. Nan, Z. H. Ni, J. Wang, Z. Zafar, Z. X. Shi and Y. Y. Wang, *J. Raman Spectrosc.*, 2013, **44**, 1018–1021.
55 T. Ozawa, *Bull. Chem. Soc. Jpn.*, 1965, **38**, 1881–1886.
56 L. Peng, W. Xiong, Y. Cai, Y. Chen, Y. He, J. Yang, J. Jin and H. Li, *Bioengineered*, 2017, **8**, 225–231.
57 X. Guo and N. Mei, *J. Food Drug Anal.*, 2014, **22**, 105–115.
58 R. F. Bader, *Acc. Chem. Res.*, 1985, **18**, 9–15.
59 M. J. Javan, *Comput. Theor. Chem.*, 2021, **1205**, 113440.
61 O. Safa, Msc., An-Najah National University, 2018.

© 2023 The Author(s). Published by the Royal Society of Chemistry